Importance of lipid–pore loop interface for potassium channel structure and function

Elwin A. W. van der Cruijsen[a,1], Deepak Nand[a,1], Markus Weingarth[a], Alexander Prokofyev[a,b], Sönke Hornig[c], Abhishek Arun Cukkemane[a], Alexandre M. J. J. Bonvin[a], Stefan Becker[d], Raymond E. Hulse[e], Eduardo Perozo[e], Olaf Pongs[b,c], and Marc Baldus[a,2]

[a]NMR Spectroscopy, Bijvoet Center for Biomolecular Research, Department of Chemistry, Faculty of Science, Utrecht University, 3584 CH Utrecht, The Netherlands; [b]Department of Physiology, Faculty of Medicine, Saarland University, 66421 Homburg, Germany; [c]Center for Molecular Neurobiology, Institute for Neural Signal Transduction, University Hospital Hamburg-Eppendorf, 20251 Hamburg, Germany; [d]Department of NMR-Based Structural Biology, Max Planck Institute for Biophysical Chemistry, 37077 Göttingen, Germany; and [e]Department of Biochemistry and Molecular Biology, Center for Integrative Science, University of Chicago, Chicago, IL 60637

Edited by Ramon Latorre, Centro Interdisciplinario de Neurociencias, Universidad de Valparaíso, Valparaíso, Chile, and approved June 21, 2013 (received for review March 22, 2013)

Potassium (i.e., K^+) channels allow for the controlled and selective passage of potassium ions across the plasma membrane via a conserved pore domain. In voltage-gated K^+ channels, gating is the result of the coordinated action of two coupled gates: an activation gate at the intracellular entrance of the pore and an inactivation gate at the selectivity filter. By using solid-state NMR structural studies, in combination with electrophysiological experiments and molecular dynamics simulations, we show that the turret region connecting the outer transmembrane helix (transmembrane helix 1) and the pore helix behind the selectivity filter contributes to K^+ channel inactivation and exhibits a remarkable structural plasticity that correlates to K^+ channel inactivation. The transmembrane helix 1 unwinds when the K^+ channel enters the inactivated state and rewinds during the transition to the closed state. In addition to well-characterized changes at the K^+ ion coordination sites, this process is accompanied by conformational changes within the turret region and the pore helix. Further spectroscopic and computational results show that the same channel domain is critically involved in establishing functional contacts between pore domain and the cellular membrane. Taken together, our results suggest that the interaction between the K^+ channel turret region and the lipid bilayer exerts an important influence on the selective passage of potassium ions via the K^+ channel pore.

membrane protein | ion channel | solid-state NMR spectroscopy

Potassium (i.e., K^+) channels are embedded in the plasma membrane to control the selective passage of potassium ions across the lipid bilayer. The channels open and close their conduction pathway by sensing changes in physicochemical parameters such as pH, ligand concentration, and membrane voltage (1). Structure–function studies on voltage-gated K^+ (Kv) channels suggested that lipid molecules are an integral part of the voltage-sensing domains, which transfer during the gating process electrical charges across the cell membrane (2–4). In some of the available Kv channel crystal structures, lipid molecules appear most densely packed against the pore domain, presumably providing an appropriate environment for the stability and the operation of the gating machinery to open and close the conduction pathway. In general, the activity of Kv pore domains is thought to be determined by the activity of two gates in series, one for activation and one for inactivation. These gates jointly control the conduction of ions through the pore (5–11). The activation gate is located at the intracellular entrance of the pore and the inactivation gate is situated toward the extracellular entrance at the selectivity filter (i.e., C-type inactivation). In addition, some potassium channels possess close to the activation gate a receptor for an N-terminal inactivating domain (i.e., N-type inactivation).

The K^+ channel pore domain is conserved across all K^+ channels. It comprises a tetrameric assembly of two transmembrane helices (helices S5 and S6 in Kv channels) connected by a pore loop region consisting of a turret, the pore helix, and the selectivity filter. Although it is now evident that structural changes at the interface between K^+ channel protein and lipid play an important role during the gating process (8, 12–16), including the coupling of voltage-sensor movements to Kv channel activation (17–20), detailed characterization of these structural changes and their implications for K^+ channel gating remain unresolved.

In this study, we addressed the structural and functional role of the protein–lipid interface at the pore loop region of a K^+ channel by using a combination of solid-state NMR (ssNMR), electrophysiological recordings, and molecular dynamics (MD) simulations. Previously, we have studied pH-induced activation and inactivation gating as well as ligand binding to KcsA-Kv1.3, a KcsA-channel variant containing the turret region of the Kv1.3 channel (21, 22). Here, we established 3D structural views of the KcsA-Kv1.3 transmembrane helices and the pore loop region before and after channel inactivation. Unexpectedly, we observed significant structural alterations in the pore loop region involving unwinding/rewinding of a helical turn at the C-terminal end of transmembrane helix 1 (TM1; S5) near the protein–lipid interface. Additional ssNMR studies reveal that the structure of this region is largely conserved in the parent KcsA channel and that mutations at the inactivation gate directly affect the structure of the pore loop region as a whole. Combined with MD simulations, our studies suggest that the interface between lipid and K^+ channel pore loop region has an important influence on the stability of the pore structure and the conformational changes associated with K^+ channel gating.

Results

We conducted ssNMR-based structural studies on the chimeric KcsA-Kv1.3 channel (21) (abbreviated henceforth as "Chim"), a construct that exclusively differs in sequence vs. WT KcsA (henceforth "WT") at amino acid residues 52 to 64 (Fig. 1). Subsequently, we compared our results to functional data on Kv1.3 channel mutants and to spectroscopic results obtained on

Author contributions: O.P. and M.B. designed research; E.A.W.v.d.C., D.N., M.W., A.P., and S.H. performed research; A.M.J.J.B., S.B., R.E.H., and E.P. contributed new reagents/analytic tools; E.A.W.v.d.C., D.N., M.W., A.P., S.H., A.A.C., A.M.J.J.B., O.P., and M.B. analyzed data; and E.A.W.v.d.C., D.N., M.W., A.P., A.M.J.J.B., S.B., E.P., O.P., and M.B. wrote the paper.

The authors declare no conflict of interest.

This article is a PNAS Direct Submission.

[1]E.A.W.v.d.C. and D.N. contributed equally to this work.

[2]To whom correspondence should be addressed. E-mail: m.baldus@uu.nl.

This article contains supporting information online at www.pnas.org/lookup/suppl/doi:10.1073/pnas.1305563110/-/DCSupplemental.

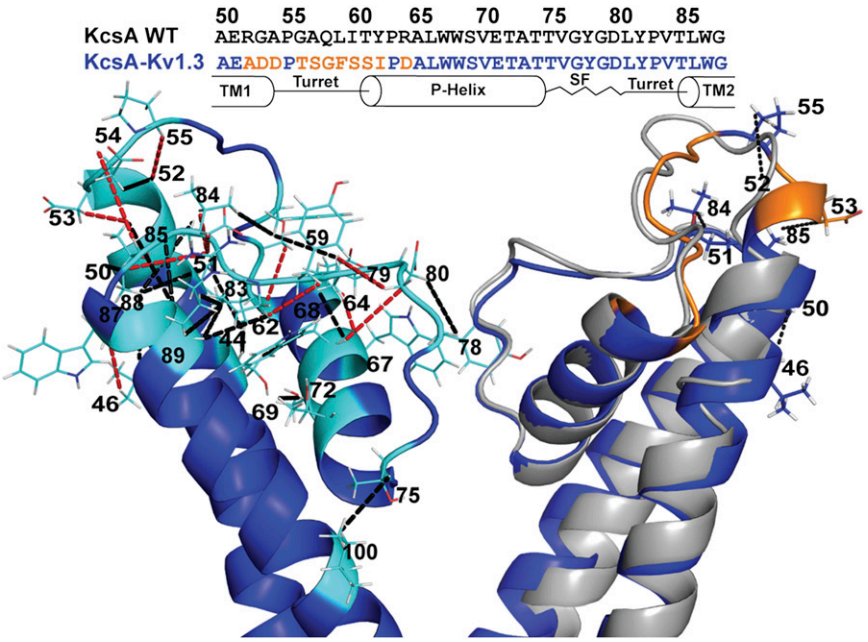

Fig. 1. SsNMR analysis of membrane-embedded Chim in the closed conductive state. (*Left*) Cartoon representation of the 3D ssNMR model of the closed state (residues Chim 22–115). Resolved CHHC restraints (highlighted in cyan) identified from the CHHC spectrum (250 μs and 500 μs ^{1}H-^{1}H mixing) that are unambiguous based on the KcsA crystal structure and the available chemical shifts are indicated by black dashed lines. Additional correlations unique for the ssNMR structure of Chim are shown by red dashed lines. (*Right*) Superposition of the Chim structural model (blue) and the KcsA crystal structure (gray) with three resolved ssNMR restraints confirming the extended α-helical turn for the chimeric channel along with their amino acid sequence comparison highlighting (orange) the 11 mutations distinguishing the turret region.

WT KcsA and KcsA mutants, which exhibit a constitutively open activation gate (23, 24) (henceforth "WTom").

Chim in the Closed Conductive State. We used an ssNMR-based hybrid strategy to establish 3D structural views of Chim before and after C-type inactivation. First, we constructed a homology model of the closed conductive state by using the crystal structure of KcsA (25) [Protein Data Bank (PDB) ID code 3EFF] and constructed a tetramer by using high ambiguity driven docking (HADDOCK) (26) (*SI Methods*). This model then served to predict and evaluate experimental CC and CHHC correlation experiments as the basis of 3D molecular structures (e.g., ref. 21). Experimental spectra were recorded on fully ^{13}C,^{15}N-labeled (Fig. S1) and on fractionally deuterated Chim (27). Resonance assignments were largely taken from published work (22). The monomeric structure of the closed pore domain (residues Chim 22–115), reconstituted in asolectin liposomes, was then calculated in Crystallography and NMR System (CNS) software (28). Distance restraints were mostly derived by comparing the experimental CHHC spectra acquired with three different mixing times (50, 250, and 500 μs) along with the CC restraints obtained from fractional deuteration studies. Overall, approximately 70% of all expected correlations were visible in CHHC spectra (*SI Methods*). Additionally, torsion angle restraints obtained from earlier chemical-shift assignments (22) were supplemented during structure calculation in CNS. The final structure, compatible with all experimental data, was characterized by more than 2,000 restraints, including 339 long-range distances (Table S1 and Fig. S2). Note that the pore loop region (residues Chim 44–90) was characterized by 156 long-range, 169 medium-range, and 148 sequential distance restraints.

The 3D structural backbone model of the closed channel state is depicted in Fig. 1 (*Left*), together with a selected set of CHHC distance restraints (Fig. 1, dashed lines). The overall channel architecture was in good agreement with the WT KcsA crystal structure (25). In detail, however, we observed significant differences with respect to the TM1 (S5) pore-loop region. First, TM1 is extended until residue Chim Asp53 and thus contains an additional turn as diagnosed by secondary chemical shifts seen earlier (8) and CHHC restraints obtained here (Fig. 1, *Right*). Second, the turret structure connecting TM1 and pore helix significantly differs from the one of the WT KcsA X-ray structure (Fig. 1, *Right*). The structural changes in this TM1-helix and turret region (henceforth "TM1T region") along with intermolecular contacts detected in our study led to a widening of the pore (Fig. S3*A*). This observation supports our previous data indicating that reduced steric hindrance in a widened Chim pore facilitates binding of the scorpion toxin Kaliotoxin (KTX) at the extracellular mouth of the channel (29).

C-Type Inactivation Involves Structural Changes in the Pore Loop. Next, we applied a similar ssNMR-based protocol to investigate structural details of open-inactivated state of the Chim channel in the lipid bilayer. Similar to WT KcsA (30), this state can be induced for the Chim channel by triggering inner gate bundle opening at low pH and reducing K^+ concentrations to less than 20 mM (8, 9). Notably, further reduction to pH 3.7 did not change our Chim ssNMR spectra, even though macroscopic and single channel measurements suggest that the apparent activation pK_a is closer to pH 4.2 for WT KcsA (31). For the analysis of the ssNMR data, an initial 3D structural model was constructed by using torsion angle restraints in channel regions known to undergo conformational changes after inactivation (8, 9). The resulting monomer fold was, in the second stage, evaluated by using long-range correlations detected in the CHHC data. The final structure (Table S1 and Fig. S2*B* provide a summary of structural restraints) revealed distinct structural rearrangements in several domains of the channel compared with the closed-conductive state (Fig. 2*A*). First, we confirmed earlier backbone chemical-shift changes in the selectivity filter residues (8, 9). In line with X-ray results on constitutively open truncated KcsA mutants (10, 23), the selectivity filter in its inactivated state is reminiscent of that of a filter under low ionic conditions [PDB ID code IK4D (30)]. Second, the absence of the observed intermolecular correlation Ile100CB–Thr74CB observed in the closed conductive state (Fig. 2*B*) and the distinct chemical-shift changes in the transmembrane helix 2 (TM2)—together with earlier results using water-edited ssNMR spectroscopy (32)—suggest that the TM2 helix rotates during K^+ channel opening, as proposed from KcsA X-ray structural analyses (23). As detailed in Fig. S3*B*, further analysis of our data suggests an opening of the activation gate by approximately

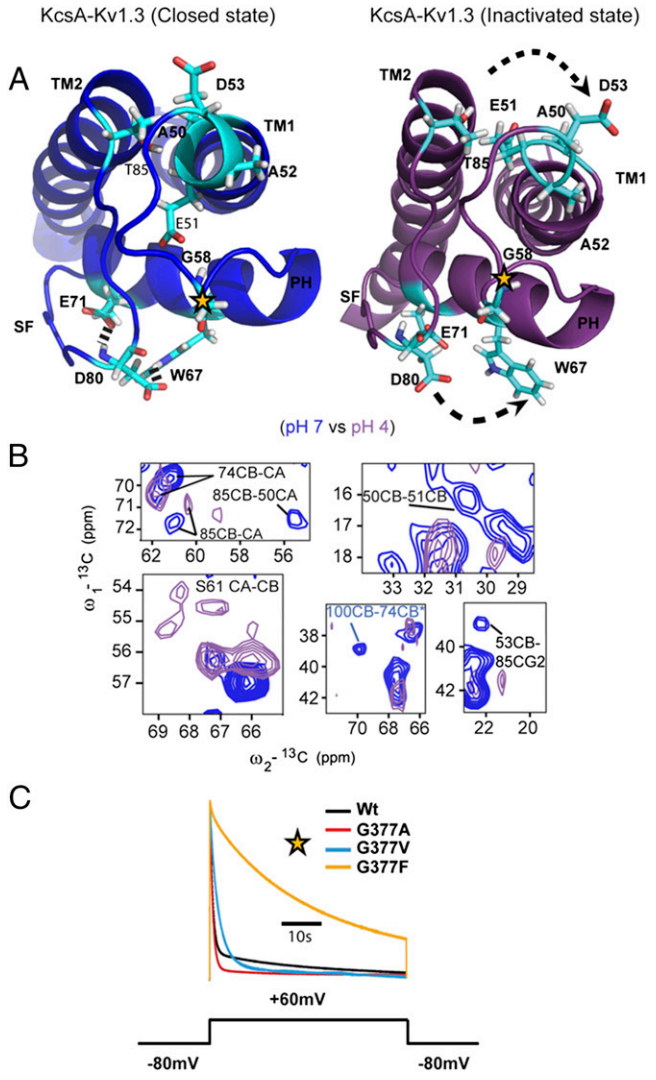

Fig. 2. ssNMR-based experiments and functional studies of a selected set of K^+ channels. (*A*) Conformational rearrangements observed for the closed (blue) and inactivated (purple) states of Chim embedded in asolectin lipid bilayer. (*B*) Spectral cutouts of (^{13}C,^{13}C) correlation spectra obtained for Chim at pH 7.0 (blue) and pH 4.0 (purple). Chemical-shift changes along with the structural restraints discerning the two channel states are shown. The absence of the intermolecular correlation of Chim 100IleCB to 74ThrCB at pH 4.0 is compatible with a reorientation of the TM2 helix. (*C*) Inactivation time courses of Kv1.3 and mutant Kv1.3 channels expressed in *Xenopus laevis* oocytes as indicated. Outward currents were elicited by the pulse protocol shown beneath the normalized current traces. Gly377 in the turret of Kv1.3 corresponds to Chim Gly58 marked by star in *A*.

23 Å, as defined by the Cα–Cα intersubunit distance at positions WT/Chim Thr112 (23), and close to the physiologically relevant opening in the full-length channel (33).

Finally, we found that several medium- and long-range correlations observed for the turret region in the closed conductive state vanished after inactivation, e.g., the one comprising Chim Asp53 to Chim Thr85 (Fig. 2*B*), whereas new correlations appeared, e.g., the one comprising Chim Thr56 to Chim Pro83 (Fig. S4*A*). In the structural ensemble, these alterations in distance and dihedral angle restraints are characteristic of a destabilization and outward rotation of the extended TM1 helix accompanied by a loss of the multipoint hydrogen-bond network of Chim Glu71, Chim Asp80, and Chim Trp67 (Fig. 2*A*). Although a distinct set of residues in the turret and the pore helix were absent in our multidimensional correlation spectra (Chim Ala50, Glu51, Asp64, and Tyr82), the results clearly indicate that conformational changes in the turret region accompany Chim inactivation. Importantly, back-titration to pH 7 fully restores the closed conductive state (Fig. S4*B*).

Previously, we have shown that Chim Gly58 in the turret region is a key residue for C-type inactivation-sensitive binding of KTX (21, 29). The conformational changes we observed between the closed and the open-inactivated state suggested that bulky residues at position 58 not only interfere with KTX binding, but also with C-type inactivation. As the Kv1.3 channel exhibits a pronounced C-type inactivation, we tested the effect of bulky side chains at position G377 (equivalent to Chim Gly58) on C-type inactivation in the Kv1.3 channel. We mutated Kv1.3 residue Gly377 to alanine, valine, and phenylalanine, respectively (Fig. 2*C*) and recorded macroscopic currents in *Xenopus* oocytes with a two-electrode voltage clamp. Although current–voltage relations, time rise to peak, and deactivation kinetics of WT and mutant Kv1.3 channels showed no significant differences (Table S2), mutating Kv1.3 G377V and especially Kv1.3 G377F markedly slowed the time course (τ_{inact}) of Kv1.3 C-type inactivation [Kv1.3, $\tau_{inact} = 0.66 \pm 0.02$ s (SEM); Kv1.3 G377A, $\tau_{inact} = 0.82 \pm 0.01$ s; Kv1.3 G377V, $\tau_{inact} = 3.61 \pm 0.20$ s; Kv1.3 G377F, $\tau_{inact} = 28.6 \pm 0.8$ s; $n = 3$–5; Fig. 2*C*). Combining the structural and functional data suggests that bulky side chains at turret residue Chim Gly58 affect the closure of the inactivation gate at the selectivity filter.

Pore Loop Structure Is Defined by a Combination of Protein–Lipid and Protein–Protein Interactions. The sequences of WT and Chim differ only by 11 aa in the turret region (Fig. 1). Structural changes observed between Chim in lipid bilayers and the crystal structure of WT KcsA could therefore be induced by changes in protein sequence and/or the presence of the lipid bilayer. To examine the influence of protein sequence, we investigated the structure of WT KcsA by ssNMR in lipid bilayers. Similar to the chimeric channel, we conducted a series of multidimensional ssNMR experiments to obtain resonance assignments and structural restraints for the WT pore loop region. We could readily assign turret residues specific for WT (Fig. S5) and generate a 3D model of WT in lipid bilayers by using a series of CHHC experiments (Fig. S6*A*). The resulting structure (Table S3) is shown in Fig. 3*A* in red, with specific medium to long-range restraints annotated in cyan and dotted lines. We compared our results vs. the 3D structure of Chim (Fig. 3*A*, *Right*, blue) and the X-ray structure of WT (Fig. 3*A*, *Right*, gray). Structures of the selectivity filter and TM1/TM2 helices are in good agreement. In contrast, we observed significant structural differences in the turret region, including an elongation of the TM1 helix for bilayer embedded WT and Chim channels. Notably, our ssNMR results are in good agreement with earlier electron paramagnetic resonance (EPR) work on WT KcsA in asolectin liposomes (31). The EPR data indicated that TM1 helix extends until WT Arg52.

Previous work has shown that mutations in the pore loop region can have a profound influence on inactivation gating of K^+ channels (13, 34–36). We investigated the influence of mutations at the pore-helix position Glu71 on the pore loop structure by comparing ssNMR data on WT KcsA (Fig. 3*B*, red) to spectra obtained on E71Q (Fig. 3*B*, green) and E71A (Fig. 3*B*, black) mutants (i.e., WTom; full data in Fig. S6*B*). As expected (36), we observed chemical-shift variations at residue WTom Asp80 that is part of a multipoint hydrogen-bond network including Glu71 in WT (35) for WTom E71Q and E71A. Interestingly, we also observed a disappearance of the extended α-helix (as diagnosed by WTom Ala50) for both gating mode mutants. Additional turret residues including WTom Ile60 and WTom Pro55 exhibited chemical shift changes and peak doubling, respectively

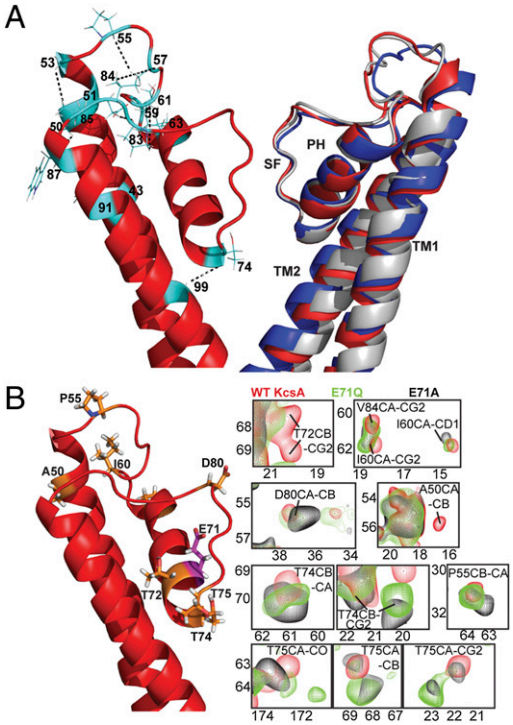

Fig. 3. (*A*) ssNMR-based structural model of membrane-embedded KcsA (WT) in the closed conductive state. (*Left*) Cartoon representation of the 3D ssNMR model of the closed state of KcsA (residues WT 22–115). Resolved CHHC restraints (highlighted in cyan) identified from the CHHC spectrum (250 μs ^{1}H-^{1}H mixing) that are unambiguous based on the ssNMR assignments. (*Right*) Superposition of the KcsA structural model (red), KcsA-Kv.1.3 (blue), and KcsA crystal structure (gray). (*B*) WTom Glu71 mutants change the conformation of the pore-loop of KcsA. (*Left*) Cartoon representation of KcsA with the mutation site E71 (purple), with residues exhibiting ssNMR shifts (blue) or peak doubling in the two mutants. (*Right*) (^{13}C,^{13}C) Correlation spectra obtained for WT (red), WTom E71Q, and WTom E71A (green and black, respectively), at pH 7.4, 50 mM [K^+] reconstituted in asolectin.

(indicated in orange on the 3D structure in Fig. 3*B*). These spectral variations extended to the pore helix (WTom Thr72) and residues in the selectivity filter (WTom Thr74/Thr75). Cross peaks for selectivity filter residues differed by approximately 2 ppm compared with correlations seen for WT KcsA in the conductive state (Fig. 3*B*, red). These observations would be compatible with increased molecular mobility around WTom Thr74/WTom Thr75. Indeed, previous MD simulations showed a considerable increase in the frequency and lifetime of WT Val76 reorientation in the WT E71Q mutant correlated with short-lived flicker states in WT E71Q single-channel recordings (36). Taken together, our results on KcsA are consistent with the view that the pore loop region functions as a functional unit that includes the extended TM1 helix coupled via the turret to the inactivation gate and extending all the way to the pore–TM2 interface. This view is in remarkable agreement with previous mutational studies in Shaker Kv channels (13).

To study the molecular details that determine the influence of lipids on the pore loop structure, we resorted to MD simulations for WT and Chim (Fig. 4) embedded in lipid bilayers. In the case of WT (Fig. 4*A*), we observed the formation of an intermolecular hydrogen bond between the WT Arg52 amidine group and WT I60CO (Fig. 4, orange lines) as well as intermolecular protein–lipid interactions (Fig. 4, magenta lines) that we suggest stabilize the helical elongation of the TM1 helix up to residue WT Gly53. The spatial proximity of the WT Arg52 amidine group to WT Ile60 was verified (Fig. 4, red lines) by a tailored ssNMR rotational resonance experiment (37) (Fig. S7). During the MD trajectory (Fig. 4*B*), we observed a remarkable correlation between helical propensity of residues WT Ala50 to WT Gly53 (Fig. 4, green) and the presence of hydrogen bonding between the WT Arg52 amidine group and WT Ile60CO (Fig. 4, orange). This view was supported by ssNMR data on the WTom E71A/Q mutants lacking the TM1T helix and exhibiting chemical-shift changes at WTom Ile60 (Fig. 3*B*). In the case of Chim, in which residues 53 and 54 are mutated (Figs. 1 and 4 *C* and *D*), we again observed intermolecular protein–lipid electrostatic interactions, namely between negatively charged Chim Asp53 and Chim Asp54 side chains and positively charged phosphatidyl-choline headgroups (Fig. 4, yellow lines) that stabilize the helical elongation of the TM1 helix up to residue Chim Asp53. Neutralizing Asp-53 and 54 (D53A, D53AD54A; Fig. 4*D*) strongly reduced α-helical propensity of residues 50 to 53, compared with Chim (Fig. 4*D*, green columns).

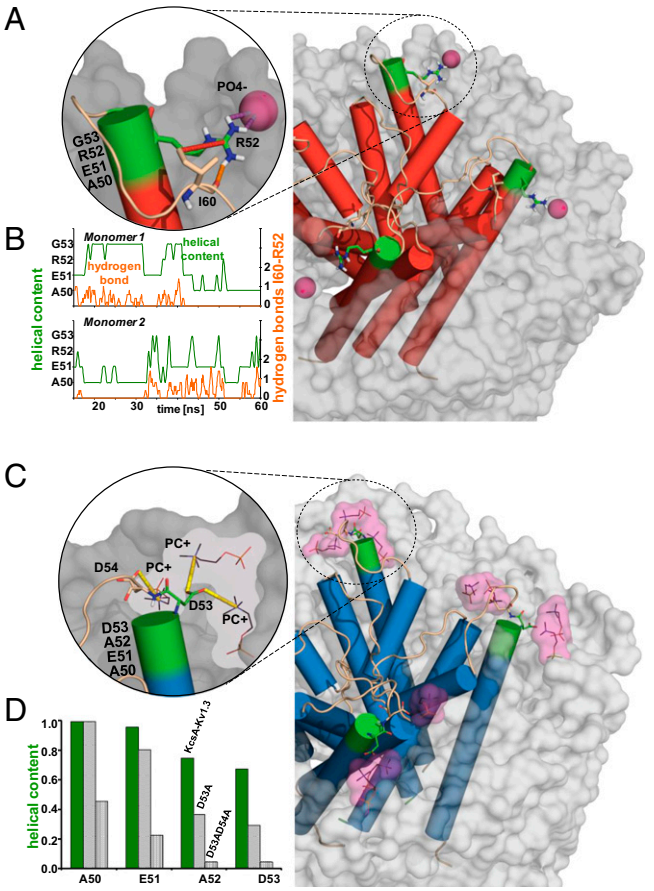

Fig. 4. (*A*) Structural snapshot of WT illustrating the intramolecular hydrogen bond between the WT Arg52 amidine group and WT Ile60CO (orange lines) and intermolecular protein–lipid interactions (magenta lines) that stabilize the helical elongation of the TM1 helix until residue WT Gly53. (*B*) Correlation of the helical propensity of residues WT Ala50 to WT Gly53 (green) and the presence of hydrogen between the WT Arg52 amidine group and WT Ile60CO (orange) evaluated for two monomers of KcsA during a 60-ns MD trajectory. (*C*) Structural snapshot of Chim illustrating the intermolecular protein–lipid electrostatic interactions between negatively charged Chim Asp53 and Chim Asp54 side chains and positively charged phosphatidylcholine headgroups (yellow lines) that stabilize the helical elongation of the TM1 helix until residue Chim Asp53. (*D*) Evaluation of the helical propensity of residues Chim Ala50 to Asp53 (green columns) and the mutants Chim D53A (dashed columns) and Chim D53A/D54A (pointed columns), averaged for monomers and 25 ns of MD trajectories.

Discussion

We have used an ssNMR-based strategy to study the 3D structure of a lipid bilayer embedded K^+ channel in its resting as well as its pH-induced inactivated states. Our major finding is an unexpected structural plasticity at the C-terminal end of the TM1-helix and the adjacent turret region, which is sensitive to lipidic environment, protein sequence, and the functional state of the K^+ channel (Fig. 5). We find that the TM1 helix unwinds when the K^+ channel enters the inactivated state and rewinds during the process of repriming into the resting state. This helical unwinding/rewinding is associated with conformational changes within the turret region and the pore helix connecting TM1 and TM2. Our results on KcsA gating mode mutants suggest an intrinsic coupling between the TM1-turret (TM1T) region and the hydrogen-bonding network in the back of the selectivity filter. The network involved in stabilizing the selectivity filter plays an important role in K^+ channel selectivity and inactivation gating. In comparison with crystal structural data (25), our ssNMR-based structural models of the Chim chimera and WT KcsA in their resting state show an extended TM1 helix toward its C-terminal end. These data are in good agreement with results of earlier EPR work suggesting an elongated TM1 helix for WT KcsA in liposomes (38).

The TM1T conformational change involves the highly conserved amino acid residue E51 (Fig. 5*A*), which plays an important role for C-type inactivation in K^+ channels. In Shaker Kv channels, mutation of E418 (equivalent to KcsA E51) to alanine boosts C-type inactivation (36). Moreover, contacts between E418 and the turret–TM2 connector region can stabilize (13) the inactivated (E418–V451, equivalent to KcsA E51–V84) or the open state (E418–G452, KcsA E51–T85). In line with the work of Larsson and Elinder (13), we observed structural changes in Chim leading to an outward rotation of TM1T and a concomitant distance increase between E51 and T85 (Fig. 2). In the KcsA channel family, E51, together with Chim S61 and Chim D64, represent peripheral protein residues, and may act as a point of interaction with the surrounding lipid bilayer. Indeed, our MD studies suggest that these pore loop residues are critically involved in stabilizing the lipid–protein interface (Fig. 5*B*, *Right*). In Kv channels, E51 fulfils a closely related role as part of a conserved residue network that extends into the S1 helix of the voltage sensor (19). In particular, the S1 T248 residue (Shaker numbering) is found in close proximity to S5 residue Y415 (Chim V48; Fig. 5) and S428 (Chim S61) in the Kv1.2-paddle crystal structure, which presumably corresponds to the open conformation.

Chim G58 (F425 in Shaker), on the contrary, is an important residue in the turret region for K^+ channel gating. When comparing the Chim structure before and after activation, substantial conformational changes have occurred around the aromatic cuff that structurally links turret residues Chim G58 and Chim F59 and amino acids around Chim D80 critical for inactivation (Fig. 5*B*, *Left*). Mutating F425 to lysine induces an electrostatic domino effect in the Shaker channel turret, ultimately affecting voltage-dependent gating (15, 39). Here, we show that mutating the equivalent residue G377 to valine and phenylalanine in the turret of the Kv1.3 channel markedly attenuates Kv1.3 C-type inactivation. It is worth noting that mutational studies on the HERG (human ether-a-go-go related gene) channel also demonstrated a functional importance of the turret region for C-type inactivation (16).

In summary, our data highlight the structural plasticity of the TM1T region at the extracellular side of the K^+ channel. In turn, this plasticity likely allows the TM1T region to engage in significant and reversible conformational changes during K^+ channel gating. Combination of our spectroscopic and MD data helped elucidate the atomic details that dictate the conformation of TM1T in a lipid environment. These studies underline the strong influence of lipids on KcsA channel gating (15, 40) and, at the same time, reveal a remarkable flexibility in maintaining lipid–protein and protein–protein contacts across different pore loop sequences. Biochemical work suggested that, during channel folding and assembly, P-loop architecture is already formed in the monomer state (41). Lipids are likely playing a fundamental role in establishing a defined structure for the monomer. In addition, lipids may also act as a cofactor in conformational changes associated with channel gating transitions (40, 42). In this process, the TM1T region could represent the cornerstone of a trajectory that leads to well defined structural alterations in pore helix, selectivity filter, and activation gate during channel activation and inactivation.

Methods

Materials and Sample Preparation. Expression, purification, and reconstitution into liposomes was done as described previously (21, 24). Reconstitution was performed at a 100/1 lipid/channel molar ratio. pH titrations were performed by thoroughly washing the proteoliposome pellet with the desired phosphate or citrate buffers, followed by 30 min ultracentrifugation at 125000 × *g* and +4 °C (9).

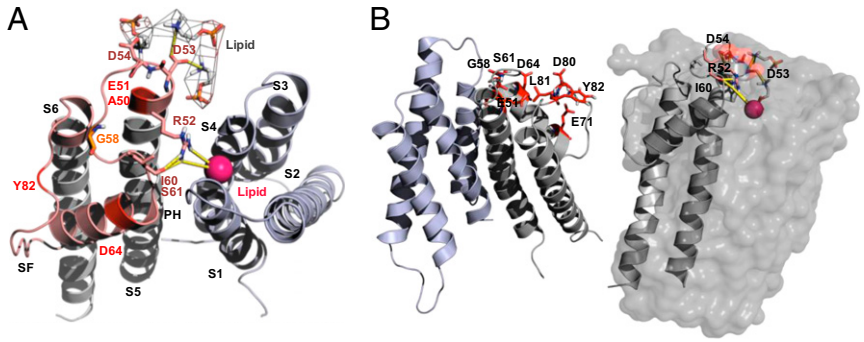

Fig. 5. Role of interfacial and turret residues in K^+ channel gating and channel stabilization. (*A*) Superposition of the inactivated state of Chim channel (gray) and the X-ray structure of the cyclic nucleotide-regulated K^+ channel MlotiK1 [light blue (45); PDB ID code 3BEH] obtained by aligning the S5–S6 subunits. Residues highlighted in red (Chim-Ala50, Glu51, Asp64, and Tyr82) exhibit strong signal attenuation of signals after inactivation whereas residues indicated in dark red undergo structural rearrangements after inactivation as shown in Fig. 2*A*. Mutation of Gly377 equivalent to Chim Gly58 (orange) strongly affects the details of C-type inactivation in Kv1.3. Residues WT Ile60, WT Ser61, and WT Asp80 undergo chemical shift changes in KcsA gating mutants. According to MD simulations, TM1T residues 52 (WT) and 53 (Chim) are critically involved in protein–protein (KcsA) as well as protein–lipid (WT and Chim) interactions that stabilize the pore loop structure. (*B*) Side views shown for the case of the MlotiK1 (*Left*) and the Chim case (*Right*) with color coding as in *A*. For the sake of clarity, only a subset of residues is depicted in *B*.

ssNMR. ssNMR experiments were conducted by using 3.2-mm or 4-mm triple-resonance (^{1}H,^{13}C,^{15}N) magic-angle-spinning (MAS) probe heads at static magnetic fields of 14.1, 16.5 and 18.8 T corresponding to proton resonance frequencies between 600 and 800 MHz (BrukerBiospin). CHHC (e.g., ref. 21) experiments were recorded at an effective sample temperature of 243 K. The CC correlation experiments were performed with an effective sample temperature varying between 273 K and 280 K. MAS frequencies used were 9.375 kHz (at 600 MHz and 700 MHz) and 12 kHz (800 MHz) for CHHC spectra and 10.92 kHz (700 MHz) for (^{13}C,^{13}C) proton-driven spin diffusion (PDSD) and phase-alternated recoupling irradiation scheme spin diffusion experiments performed under weak coupling conditions (43). A ^{1}H field strength of 83.3 kHz was used for 90° pulses and small phase incremental alternation 64 (44) decoupling during evolution and acquisition. CHHC experiments were acquired with ^{1}H-^{1}H mixing times of 50, 250, and 500 μs by using an initial cross-polarization (CP) step of 700 μs and CP steps of 80 μs enclosing the proton mixing step to select for one bond (C-H) magnetization transfer. Mixing times of 20 ms or 30 ms were used to obtain intraresidue (^{13}C,^{13}C) correlations in PDSD experiments.

MD. MD simulations were carried out using the Groningen Machine for Chemical Simulations (GROMACS) simulations package, version 4.5.3 (45), with the Groningen Molecular Simulation computer program package (GROMOS53a6) force field (46). The simulation systems were represented by the atomic models of Chim and WT KcsA, embedded in a bilayer in an aqueous solution of KCl. Potassium and chloride ions were added to electrostatically neutralize the systems and to mimic 80 mM KCl solutions. The KcsA starting structure was derived from crystal structure 3EFF (PDB) (25) to probe spontaneous helical elongation of TM1, the Chim starting structure from our ssNMR-based structure model. Mutations in the Chim model were introduced with Pymol (Delano Scientific). All systems were simulation at constant-pressure for at least 25 ns.

Electrophysiology. The expression of Kv1.3 WT and mutant channels in the *Xenopus* oocyte expression system was as described previously (31). Activation, deactivation time courses, and voltage-conductance relations were measured with test pulses of 100 ms starting from a holding potential of −100 mV. For measurement of Kv1.3 inactivation, we used long test-pulse durations of 60 s at test potentials of +60 mV, where Kv1.3 channels are completely activated. Inactivation time courses and recovery from inactivation were evaluated by using HEKA-PULSEFIT in combination with KaleidaGraph software. Statistical significance was tested by Student *t* test.

ACKNOWLEDGMENTS. We thank Karin Giller and Iris Ohmert for excellent technical support and Dr. C. Ader for initial studies on this project. This work was supported by Nederlandse Organisatie voor Wetenschappelijk Onderzoek Grants 700.56.442 (to A.M.J.J.B.), 700.11.344 (to M.B.), and 700.58.102 (to M.B.); Max Planck Society; Deutsche Forschungsgemeinschaft Grants Be 2345/5-1, Po137, 40-1, and 41-1; European Union Contract Bio-NMR 261863; National Institutes of Health/National Institute of General Medical Sciences Grant GM087519; the Hertie Foundation; and a Federation of European Biochemical Societies long-term fellowship (to M.W.).

1. Hille B (2001) *Ionic Channels of Excitable Membranes* (Sinauer, Sunderland, MA), 3rd Ed.
2. Schmidt D, Jiang Q-X, MacKinnon R (2006) Phospholipids and the origin of cationic gating charges in voltage sensors. *Nature* 444(7120):775–779.
3. Long SB, Tao X, Campbell EB, MacKinnon R (2007) Atomic structure of a voltage-dependent K+ channel in a lipid membrane-like environment. *Nature* 450(7168): 376–382.
4. Bezanilla F (2008) How membrane proteins sense voltage. *Nat Rev Mol Cell Biol* 9(4): 323–332.
5. Baukrowitz T, Yellen G (1995) Modulation of K+ current by frequency and external [K+]: A tale of two inactivation mechanisms. *Neuron* 15(4):951–960.
6. Baukrowitz T, Yellen G (1996) Use-dependent blockers and exit rate of the last ion from the multi-ion pore of a K+ channel. *Science* 271(5249):653–656.
7. Panyi G, Deutsch C (2006) Cross talk between activation and slow inactivation gates of Shaker potassium channels. *J Gen Physiol* 128(5):547–559.
8. Ader C, et al. (2008) A structural link between inactivation and block of a K+ channel. *Nat Struct Mol Biol* 15(6):605–612.
9. Ader C, et al. (2009) Coupling of activation and inactivation gate in a K+-channel: Potassium and ligand sensitivity. *EMBO J* 28(18):2825–2834.
10. Cuello LG, et al. (2010) Structural basis for the coupling between activation and inactivation gates in K(+) channels. *Nature* 466(7303):272–275.
11. Panyi G, Deutsch C (2007) Probing the cavity of the slow inactivated conformation of shaker potassium channels. *J Gen Physiol* 129(5):403–418.
12. Liu Y, Jurman ME, Yellen G (1996) Dynamic rearrangement of the outer mouth of a K+ channel during gating. *Neuron* 16(4):859–867.
13. Larsson HP, Elinder F (2000) A conserved glutamate is important for slow inactivation in K+ channels. *Neuron* 27(3):573–583.
14. Valiyaveetil FI, Zhou Y, MacKinnon R (2002) Lipids in the structure, folding, and function of the KcsA K+ channel. *Biochemistry* 41(35):10771–10777.
15. Marius P, et al. (2008) Binding of anionic lipids to at least three nonannular sites on the potassium channel KcsA is required for channel opening. *Biophys J* 94(5): 1689–1698.
16. Wang DT, Hill AP, Mann SA, Tan PS, Vandenberg JI (2011) Mapping the sequence of conformational changes underlying selectivity filter gating in the K(v)11.1 potassium channel. *Nat Struct Mol Biol* 18(1):35–41.
17. Broomand A, Männikkö R, Larsson HP, Elinder F (2003) Molecular movement of the voltage sensor in a K channel. *J Gen Physiol* 122(6):741–748.
18. Gandhi CS, Clark E, Loots E, Pralle A, Isacoff EY (2003) The orientation and molecular movement of a k(+) channel voltage-sensing domain. *Neuron* 40(3):515–525.
19. Lee S-Y, Banerjee A, MacKinnon R (2009) Two separate interfaces between the voltage sensor and pore are required for the function of voltage-dependent K(+) channels. *PLoS Biol* 7(3):e47.
20. Catterall WA (2010) Ion channel voltage sensors: Structure, function, and pathophysiology. *Neuron* 67(6):915–928.
21. Lange A, et al. (2006) Toxin-induced conformational changes in a potassium channel revealed by solid-state NMR. *Nature* 440(7086):959–962.
22. Schneider R, et al. (2008) Solid-state NMR spectroscopy applied to a chimeric potassium channel in lipid bilayers. *J Am Chem Soc* 130(23):7427–7435.
23. Cuello LG, Jogini V, Cortes DM, Perozo E (2010) Structural mechanism of C-type inactivation in K(+) channels. *Nature* 466(7303):203–208.
24. Cuello LG, et al. (2010) Design and characterization of a constitutively open KcsA. *FEBS Lett* 584(6):1133–1138.
25. Uysal S, et al. (2009) Crystal structure of full-length KcsA in its closed conformation. *Proc Natl Acad Sci USA* 106(16):6644–6649.
26. de Vries SJ, van Dijk M, Bonvin AM (2010) The HADDOCK Web server for data-driven biomolecular docking. *Nat Protoc* 5(5):883–897.
27. Nand D, Cukkemane A, Becker S, Baldus M (2012) Fractional deuteration applied to biomolecular solid-state NMR spectroscopy. *J Biomol NMR* 52(2):91–101.
28. Brünger AT, et al. (1998) Crystallography & NMR system: A new software suite for macromolecular structure determination. *Acta Crystallogr D Biol Crystallogr* 54(pt 5): 905–921.
29. Zachariae U, et al. (2008) The molecular mechanism of toxin-induced conformational changes in a potassium channel: Relation to C-type inactivation. *Structure* 16(5): 747–754.
30. Zhou YF, Morais-Cabral JH, Kaufman A, MacKinnon R (2001) Chemistry of ion coordination and hydration revealed by a K+ channel-Fab complex at 2.0 A resolution. *Nature* 414(6859):43–48.
31. Chakrapani S, Cordero-Morales JF, Perozo E (2007) A quantitative description of KcsA gating I: Macroscopic currents. *J Gen Physiol* 130(5):465–478.
32. Ader C, et al. (2009) Structural rearrangements of membrane proteins probed by water-edited solid-state NMR spectroscopy. *J Am Chem Soc* 131:170–176.
33. Uysal S, et al. (2011) Mechanism of activation gating in the full-length KcsA K+ channel. *Proc Natl Acad Sci USA* 108(29):11896–11899.
34. Yifrach O, MacKinnon R (2002) Energetics of pore opening in a voltage-gated K(+) channel. *Cell* 111(2):231–239.
35. Cordero-Morales JF, et al. (2006) Molecular determinants of gating at the potassium-channel selectivity filter. *Nat Struct Mol Biol* 13(4):311–318.
36. Chakrapani S, et al. (2011) On the structural basis of modal gating behavior in K(+) channels. *Nat Struct Mol Biol* 18(1):67–74.
37. Weingarth M, et al. (2012) Supramolecular structure of membrane-associated polypeptides by combining solid-state NMR and molecular dynamics simulations. *Biophys J* 103(1):29–37.
38. Perozo E, Cortes DM, Cuello LG (1998) Three-dimensional architecture and gating mechanism of a K+ channel studied by EPR spectroscopy. *Nat Struct Biol* 5(6):459–469.
39. Broomand A, Österberg F, Wardi T, Elinder F (2007) Electrostatic domino effect in the Shaker K channel turret. *Biophys J* 93(7):2307–2314.
40. Weingarth M, et al. (2013) Structural determinants of specific lipid binding to potassium channels. *J Am Chem Soc* 135(10):3983–3988.
41. Gajewski C, Dagcan A, Roux B, Deutsch C (2011) Biogenesis of the pore architecture of a voltage-gated potassium channel. *Proc Natl Acad Sci USA* 108(8):3240–3245.
42. Xu YP, Ramu Y, Lu Z (2008) Removal of phospho-head groups of membrane lipids immobilizes voltage sensors of K+ channels. *Nature* 451(7180):826–829.
43. Seidel K, et al. (2004) Protein solid-state NMR resonance assignments from (13C, 13C) correlation spectroscopy. *Phys Chem Chem Phys* 6:5090–5093.
44. Fung BM, Khitrin AK, Ermolaev K (2000) An improved broadband decoupling sequence for liquid crystals and solids. *J Magn Reson* 142(1):97–101.
45. Hess B, Kutzner C, van der Spoel D, Lindahl E (2008) GROMACS 4: Algorithms for highly efficient, load-balanced, and scalable molecular simulation. *J Chem Theory Comput* 4:435–447.
46. Soares TA, et al. (2005) An improved nucleic acid parameter set for the GROMOS force field. *J Comput Chem* 26(7):725–737.